Impact of Human Blockage on Dynamic Indoor Multipath Channels at 27 GHz

Robbert Schulpen, Laurens A. Bronckers, *Member, IEEE*, A. Bart Smolders, *Senior Member, IEEE*, and Ulf Johannsen, *Member, IEEE*

***Abstract*— Human blockage and its dynamics are potential challenges for millimeter-wave (mm-wave) mobile communication. This article presents the results of wideband measurements at 27 GHz with one human blocker close by a dynamic mobile terminal (MT) as well as one or multiple dynamic human blockers further away from an MT. The measured human blockage loss is largest when the direct path (DP) in a line-of-sight (LOS) is blocked, but this loss is limited by other multipath components (MPCs). For nonline-of-sight (NLOS) channels, it is shown that human blockage loss is typically negligible. The presented measurement results show that human blockage loss in multipath channels is much smaller than that reported in diffraction- and measurement-based models, which neglect or minimize the contribution of all MPCs other than the DP. This suggests that the multipath nature of the indoor wireless channel highly limits the impact of human blockage.**

***Index Terms*— Channel dynamics, channel sounding, delay spread (DS), human blockage, indoor measurements, millimeter-wave (mm-wave) propagation, path loss (PL).**

I. Introduction

THE global mobile network data traffic has grown over 50% per year since 2014 and it is expected that the fifth generation (5G) of wireless communication will account for 54% of this data traffic in 2026 [1]. The millimeter-wave (mm-wave) band is expected to play a vital role in providing high-speed and high-capacity networks for future mobile applications in 5G. The 24.25–27.5 GHz, 37–43.5 GHz, and 66–71 GHz bands have been identified at the World Radio Conference 2019 for implementation of the terrestrial part of International Mobile Telecommunications [2]. Moreover, the European Commission has implemented a decision for the availability and efficient use of the 24.25–27.5 GHz band in the European Union for wireless broadband communication services [3], [4]. The use of these higher frequencies in 5G poses several challenges, which include directional communication, rapid channel fluctuations, and severe shadowing [5]. Human blockage is a potential cause of rapid channel fluctuations and shadowing, and its impact on the 27 GHz channel is investigated in this article.

Manuscript received 1 June 2021; revised 10 February 2022; accepted 15 March 2022. Date of publication 29 March 2022; date of current version 6 October 2022. *(Corresponding author: Robbert Schulpen.)*

The authors are with the Department of Electrical Engineering, Eindhoven University of Technology, 5600 MB Eindhoven, The Netherlands (e-mail: r.schulpen@tue.nl).

Color versions of one or more figures in this article are available at https://doi.org/10.1109/TAP.2022.3161692.

Digital Object Identifier 10.1109/TAP.2022.3161692

An overview of human blockage models is given in [6]. Human blockage is often modeled by diffraction-based models, which are based on either the geometrical theory of diffraction or uniform geometrical theory of diffraction and use simplified shapes such as screens and cylinders to model the human body. These models are often verified by measurements of human blockers walking in straight lines in between directional antennas, which are separated by a short distance to minimize the impact of the environment on the measurements [7]–[10]. In [11]–[13], measurement-based human blockage models are reported. These models are derived from human blockage measurements over short distances using either directional antennas or neglecting multipath components (MPCs) other than the direct path (DP). These diffraction- and measurement-based models neglect or limit the impact of MPCs other than the DP. This could result in an overestimation of human blockage loss when these blockage models are applied in stochastic models of multipath channels.

This article presents channel sounding results of an extensive measurement campaign at 27 GHz, which shows the impact of human blockage on dynamic indoor multipath channels between an access point (AP) and a mobile terminal (MT) for the first time. This is important because the human blockage models available in the literature do not include the effect of MPCs on the perceived human blockage loss. Two measurement scenarios are explored in this article: 1) a dynamic MT with a close by human blocker and 2) a static MT with one or multiple human blockers. The measured human blockage loss provides deterministic insight into the channel and its dynamics and is compared to the human blockage loss reported in the literature to show how it is affected by the multipath environment. The impact of human blockage on the fit of the measured path loss (PL) to the close-in PL model (CI-model) is determined for scenario 1. Furthermore, the effect of human blockage on the measured rms delay spread (DS) is shown. The measurements are aggregated to approximate the omnidirectional channel response and are further analyzed to provide insight into the impact of human blockage on directional channels.

The key contributions of this work can be summarized as follows:

1) results and analysis of the first extensive measurement campaign on dynamic indoor human blockage at 27 GHz;

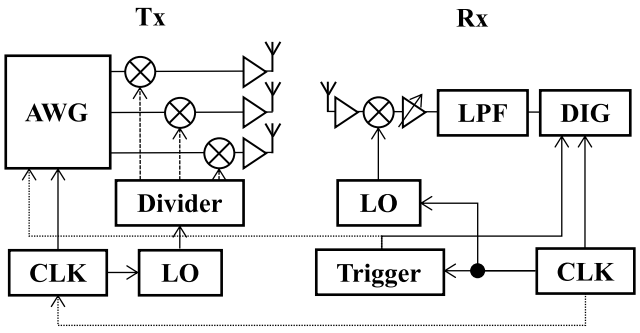

Fig. 1. Block diagram of MISO channel sounder.

TABLE I
CHANNEL SOUNDER SETTINGS AND PARAMETERS

Parameter	Value
# Tx channels T	3
# Rx channels	1
EIRP per channel	29 dBm
MLS length	4095 chips
Carrier frequency	27 GHz
Chip rate	399.90234375 Mcps
Trigger rate	4.8828125 kHz
Chip resolution	2.5 ns
Unambiguous range	3 km
Dynamic range	20 dB
Maximum measurable PL	143 dB
Measurement interval	0.2 s
# Snapshots per measurement point N_s	50

2) analysis of the impact of human blockage on PL and DS statistics;
3) analysis of the impact of human blockage on both directional and approximated omnidirectional channels.

The remainder of this article is organized as follows. The measurement setup is described in Section II. In Section III, the measurement scenarios are described. The measurement results of scenarios 1 and 2 are presented in Sections IV and V, respectively. This article is concluded in Section VI.

II. MEASUREMENT SETUP

A. Hardware

A 3 × 1 multiple-input–single-output (MISO) channel sounder has been developed at the Eindhoven University of Technology. A block diagram of the channel sounder is shown in Fig. 1 and an overview of its settings and parameters is given in Table I.

Three BPSK-modulated maximum-length sequences (MLSs) with 4095 chips each are transmitted sequentially by an arbitrary waveform generator (AWG) at a rate of 399.90234375 Mcps via three distinct transmit channels. The MLS is upconverted to 27 GHz and amplified to 25 dBm, where the carrier is provided by a local oscillator (LO). The 20 dB attenuators are used in the indoor campaign to limit the transmit power to 5 dBm. Vertically polarized standard gain horn antennas with a gain of 24 dBi, E-plane half-power beamwidth (HPBW) of 10°, and an H-plane HPBW of 11° are used at the transmitter (Tx), which results in a maximum effective isotropic radiated power (EIRP) of 29 dBm per channel. A vertically polarized 3 dBi omnidirectional antenna with a 45° E-plane HPBW is used at the receiver (Rx). The received signal is amplified by a low-noise amplifier with 48 dB gain and 4 dB noise figure and downconverted to an intermediate frequency of 800 MHz. The signal is then amplified by an 8 dB hybrid amplifier, low-pass filtered (LPF), and digitized at a rate of 3.2 GS/s by a digitizer (DIG).

The Tx and Rx equipment is mounted in and on top of mobile carts. A 360° camera at the Rx cart records a video at 30 frames/s, which is used for synchronization and analysis of the measurements. A measurement is taken every 0.2 s. Every measurement point consists of 50 snapshots of the channel at a trigger rate of 4.8828125 kHz, where each snapshot includes a record of all three sequentially transmitted MLS.

B. Synchronization

Rubidium clocks (denoted as CLK in Fig. 1) are used for frequency and temporal synchronization between the Tx and the Rx. Before the start of the measurement campaign, the Tx is triggered by a trigger module to start transmitting a distinct repetitive sequence at each Tx channel, which consists of multiple copies of the corresponding MLS and zeros. The zeros are added to prevent transmission of a channel during the time slots a different channel is transmitting an MLS, which enables sequential transmission of the three Tx channels.

The wired connection between the two rubidium clocks is removed just before the start of the measurement campaign. The DIG is triggered by the trigger module before every snapshot to provide temporal synchronization. The drift between the Tx and the Rx is approximately linear when the rubidium clocks are disconnected [14]. A linear fit is applied between the wired back-to-back measurements at the start and end of the measurement campaign to determine the approximate drift for each measurement, which is compensated for to obtain accurate absolute delays. During the 7 h measurement campaign described in this article, 12 line-of-sight (LOS) measurements with known Tx–Rx distance are taken to estimate the mean and maximum error that the linear drift assumption entails. The mean and maximum errors for these measurements are 2 and 8 ns, respectively, which correspond to errors of 0.6 and 2.4 m, respectively.

C. Postprocessing

The digitized signal with low intermediate frequency is downconverted to baseband, LPF, and resampled to eight times the chip rate, which enables all further processing with exactly eight samples per chip. The calibration method described in [15] is applied to remove the system response from the measured channel response, using a back-to-back measurement between each Tx channel and the Rx. A compensation for the antenna gains is then applied to obtain the channel impulse responses. The power-delay-profile (PDP) for each

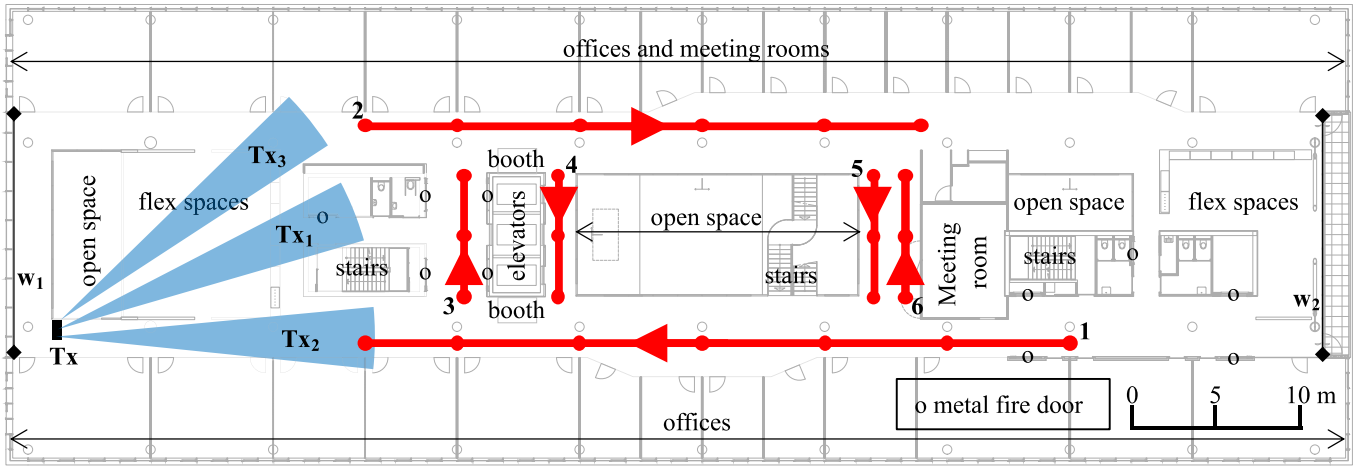

Fig. 2. Floor plan of measurement scenario 1, depicting the three Tx beams and six Rx tracks. The direction of movement is indicated by the red arrows and the synchronization points are depicted by red dots. The open spaces indicate the areas where no flooring is present.

channel is calculated as

$$p_t(\tau) = \frac{1}{N_s}\sum_{k=1}^{N_s}\left|h_t^k(\tau)\right|^2 \tag{1}$$

where τ is the delay index, $N_s = 50$ is the number of snapshots, and $h_t^k(\tau)$ is the channel impulse response of the channel of transmit beam $\mathrm{Tx_t}$ (with $\mathrm{t} = 1, 2, 3$) and snapshot k. The PDP of the aggregate channel between the three Tx channels and the Rx is calculated as

$$p^{tot}(\tau) = \sum_{t=1}^{T} p_t(\tau) \tag{2}$$

where $T = 3$ is the number of transmit channels. The aggregate channel is denoted by superscript tot in this article and approximates the omnidirectional channel as will be shown in Section III. Equation (2) implements the summation of directional channels to acquire the aggregate channel response, a method also used in [16] and [17]. This method requires sufficient spatial isolation between the Tx beams to avoid duplicate counting of paths. An alternative method [18], [19] of using the maximum instead of the sum over the directional channels eliminates the isolation requirement but suffers from not counting paths at delay instances where another stronger path is present via a different Tx beam. It will be shown in Section III that the isolation is sufficient for the considered measurement scenarios to use the summation method.

A dynamic threshold of 20 dB below the PDP peak value, as also used in [20]–[22], is applied to exclude potential spurious peaks that remain after calibration. A fixed threshold is defined at -150 dB to exclude noise. All delay indices, τ_{TH}, of a PDP above the threshold can then be defined as

$$\left\{\tau_{TH} \in \tau \wedge p^{tot}(\tau_{TH}) > TH\right\} \tag{3}$$

where TH is the maximum of the dynamic and fixed thresholds. The PL of the aggregate channel is calculated as

$$\mathrm{PL^{tot}} = -10\log_{10}\left(\sum_{\tau_{TH}} p^{tot}(\tau_{TH})\right). \tag{4}$$

The DS is defined as

$$\mathrm{DS^{tot}} = \sqrt{\frac{\sum_{\tau_{TH}}\left((\tau_{TH} - T_D - \tau_M)^2 p^{tot}(\tau_{TH})\right)}{\sum_{\tau_{TH}} p^{tot}(\tau_{TH})}} \tag{5}$$

where

$$T_D = \frac{\sum_{\tau_{TH}} \tau_{TH}\, p^{tot}(\tau_{TH})}{\sum_{\tau_{TH}} p^{tot}(\tau_{TH})} - \tau_M \tag{6}$$

and τ_M is the delay corresponding to the first path in the PDP [23]. The formulas for the PL and DS of the separate channels between the Tx and Rx can be obtained by replacing the superscript tot by the subscript t in (4)–(6).

III. Measurement Scenarios

Measurements are performed at floor 9 of the flux building at the Eindhoven University of Technology campus to investigate the impact of human blockage on the indoor multipath channel. A floor plan is shown in Fig. 2 and pictures of the measurement environment can be seen in Fig. 3. This floor is a modern open office environment with two long corridors, glass-walled offices and meeting rooms at the sides, flexible workspaces at both ends, an open space at its center, and concrete floors. There are large windows at both ends of the corridors, denoted by $\mathrm{w_1}$ and $\mathrm{w_2}$. Besides the elevators, metal fire doors that are countersunk into the walls are potentially good reflectors. The Tx, which acts as an AP, is placed at one end of a long corridor and each Tx beam is directed toward one of the three corridors that are visible from the Tx site. The Rx represents an MT in the channel. The Tx antenna height is 1.8 m and the Rx antenna height is 1.5 m. Two measurement scenarios are explored: 1) a dynamic MT with a close by human blocker and 2) a static MT with one or multiple human blockers. Scenario 1 allows for the measurement of human blockage for an MT at many locations in the office environment, where the blocker is within 0.4–0.8 m from the MT. Scenario 2 shows the impact of one or multiple human blockers further away from the MT in a multipath channel.

(a)

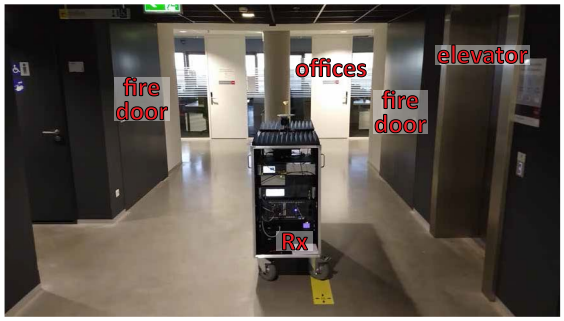

(b)

(c)

Fig. 3. Photographs of measurement environment. (a) View from behind the Tx is shown. (b) Rx at the center of track 3 is depicted. (c) Image of the Rx camera taken at three quarters of track 2 is shown.

A. Scenario 1: Dynamic MT With Close by Human Blocker

The first measurement scenario that is investigated is the dynamic MT with a close by person that can potentially block (part of) the AP-MT channel. This potential human blocker pushes or pulls the Rx cart and is 1.9 m tall. Five blocker positions are defined in Fig. 4 with respect to the walking direction indicated by a gray arrow. b_0 represents the unblocked reference case, where the operator is completely below the surface of the cart. b_1 represents a blocker at the back with the operator walking upright. b_2 is the front blocker position, where the operator pulls the cart forward in upright posture. b_3 and b_4 are the left- and right-side blockers, respectively, where the operator is slightly off-center from the antenna, because of practical limitations when pushing the cart from the side. The distance between the Rx antenna and the human blocker is approximately 0.8 m for b_1 and b_2 and 0.4 m for b_3 and b_4.

An overview of this measurement scenario is shown in Fig. 2. The Rx is moved three times along each of the six

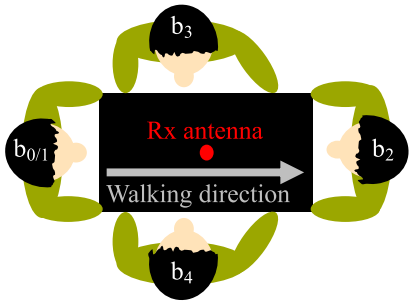

Fig. 4. Illustration of the five measured human blocker positions for scenario 1, where blocker position b_0 depicts the unblocked case with the operator completely below the surface of the cart.

indicated tracks for all five blocker positions. The direction of movement is indicated by the red arrows. Track 1 is completely in LOS, while tracks 2–6 are entirely in nonline-of-sight (NLOS). The measurement locations are synchronized with the recorded video via timestamps. The Tx–Rx distance is determined at all positions indicated by the red dots in Fig. 2. The Tx–Rx distance is then calculated for all measurement points along the tracks via interpolation between the red dots, assuming a constant velocity of the Rx cart.

The aggregate channel approximates the omnidirectional channel between the Tx and Rx because the three Tx beams cover the three corridors with their HPBW and the spatial isolation between the Tx beams is more than 7 dB for all angles of departure in the direction of the corridors. This spatial isolation is sufficient and significantly larger than the spatial isolation in case of the commonly used channel sounding practice of rotating a horn antenna in steps of one HPBW [16], [17], [24].

B. Scenario 2: Static MT With One or Multiple Human Blockers

A second set of experiments is conducted where one or multiple dynamic potential human blockers (1HB/MHB) are walking in an area around a static MT. Fig. 5 shows this measurement scenario with the Rx located at LOS location s_{LOS} and NLOS location s_{NLOS}. In this experiment, the 1HB walks through the corridors along the depicted lines to cover the main part of the area around the Rx. This deterministic approach is used to approximate the human blockage distribution for one blocker in the corresponding areas. The tracks are color-coded, where, for example, $1HB_{LOS}$-PT indicates the measurement set of one human blocker walking along the purple track for static LOS location s_{LOS}. The MHB measurements are conducted with multiple people walking randomly in the gray area in case of s_{LOS} (denoted by MHB_{LOS}) and yellow area in case of s_{NLOS} (denoted by MHB_{NLOS}). This shows the impact of multiple potential human blockers in the channel compared to one or no blocker. Six people are present in the MHB_{LOS} measurements, which is a realistic number of people walking through this office corridor at the same time. Only three people are part of the MHB_{NLOS} measurements because of the smaller area.

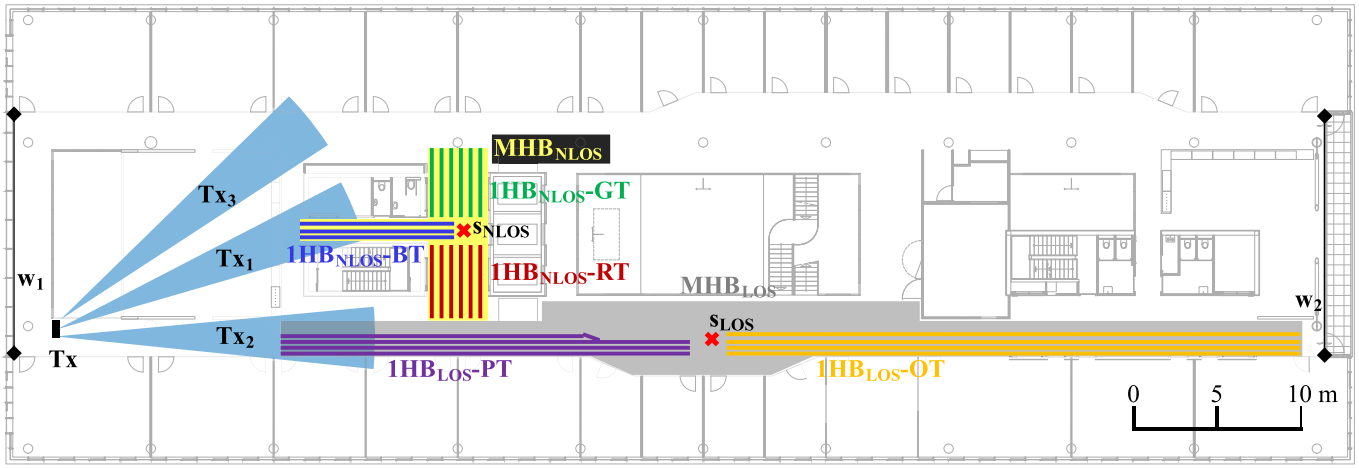

Fig. 5. Overview of measurement scenario 2 with the Rx at static locations s_{LOS} and s_{NLOS}. The tracks along which the 1HB walks are depicted by straight lines and the areas in which the MHB walk are shown colored.

IV. Results of Scenario 1: Dynamic MT With Close by Human Blocker

For scenario 1 in Fig. 2, the human blockage loss is determined along each track for the blocker positions shown in Fig. 4. First, the measurement results along the tracks are discussed to provide deterministic insight into the measured channels. The statistics of the measured human blockage loss are provided to show its general impact on the multipath channel. The fit of the PL to the CI-model is discussed to show how it is impacted by human blockage and the impact of human blockage on the DS along the tracks is shown. Finally, the impact of human blockage on the corresponding directional channels is discussed.

A. Comparison of Human Blockage Loss per Track

A comparison of the blocker positions b_1–b_4 with the unblocked position b_0 provides deterministic insight into the human blockage loss per track. The three repeated measurement sets of PL^{tot} are combined in one set for each track and blocker position. A uniformly weighted moving average with a window of ±0.5 m around every measurement point is then applied to obtain the average PL^{tot}. The human blockage loss is then calculated as the difference between the average PL^{tot} with respect to the average PL^{tot} of b_0 for each blocker position b_1–b_4. Fig. 6 shows the human blockage loss along each track of scenario 1. The corresponding PDPs, video footage, and individual contributions of each beam Tx_t are analyzed, but not all shown for the sake of brevity.

1) LOS Track 1: The largest blockage loss is observed in Fig. 6(a) for blocker position b_2 along LOS track 1. This blocker position is directly within the DP between the Tx and the Rx, which results in a maximum blockage loss of 16 dB. Large fluctuations in blockage loss as a function of position as well as negative blockage loss can be observed. Their origin can be explained using the corresponding PDPs.

The normalized PDP $p^{tot}(\tau)$ of an unblocked measurement (b_0) in the middle of track 1 is shown in Fig. 7, which shows the distinct MPCs in this measurement. Several distinct paths are visible besides the DP, which are established via reflections from windows w_1 and w_2 (see Fig. 2). These reflected paths are denoted as WR_r, where r indicates the order in which the window reflections of the corresponding path occur. The paths WR_2, $WR_{2,1}$, and $WR_{2,1,2}$ are above the 20 dB threshold at some parts of track 1. WR_2 is sometimes even stronger than the DP for b_0, which is due to multipath fading. Multipath fading between paths within both the DP and WR_2, which cannot be distinguished at the chip resolution of 2.5 ns, causes fluctuations in the measured PL^{tot} and human blockage loss. WR_2 is relatively strong at the start of track 1, where its propagation distance is smallest, resulting in a relatively low blockage loss there when the DP is blocked by b_2. Blocker position b_1, which mainly affects WR_2, results in a relatively large blockage loss of up to 8 dB at the parts of the track where WR_2 is stronger than the DP for b_0. The negative blockage loss can also be explained by changes in multipath fading due to the different blocker positions.

2) NLOS Tracks 2–6: For NLOS tracks 2–6, the maximum measured blockage loss is 5 dB [see Fig. 6(b)–(f)]. The largest blockage events along these tracks can be explained by comparison with the scenario layout in Fig. 2. The largest blockage for track 2 occurs at the beginning of this track, where paths via the glass-walled offices at the side are blocked by blocker b_3 at the left of the Rx cart, which results in a blockage loss of up to 4 dB. Beam Tx_2 is optimum at the beginning of track 3 via a reflected path from the metal fire door at the right of this track, which is blocked by blocker position b_4 and results in a 2–3 dB blockage loss. Paths via beam Tx_1 are strongest at the middle of this track, where blockage by b_3 results in up to 4 dB loss. Furthermore, blockers b_1 and b_4 cause up to 3 dB loss by blocking reflected paths via the elevator. A maximum blockage of 5 dB occurs at the end of track 3, where paths via beam Tx_3 are blocked.

Track 4 shows the smallest overall blockage loss. The PL is relatively high along this track and many paths from beam Tx_2 with similar magnitude contribute to the channel. Thus, blockage by all positions can be effectively compensated by paths from other directions. Beam Tx_2 is optimum along

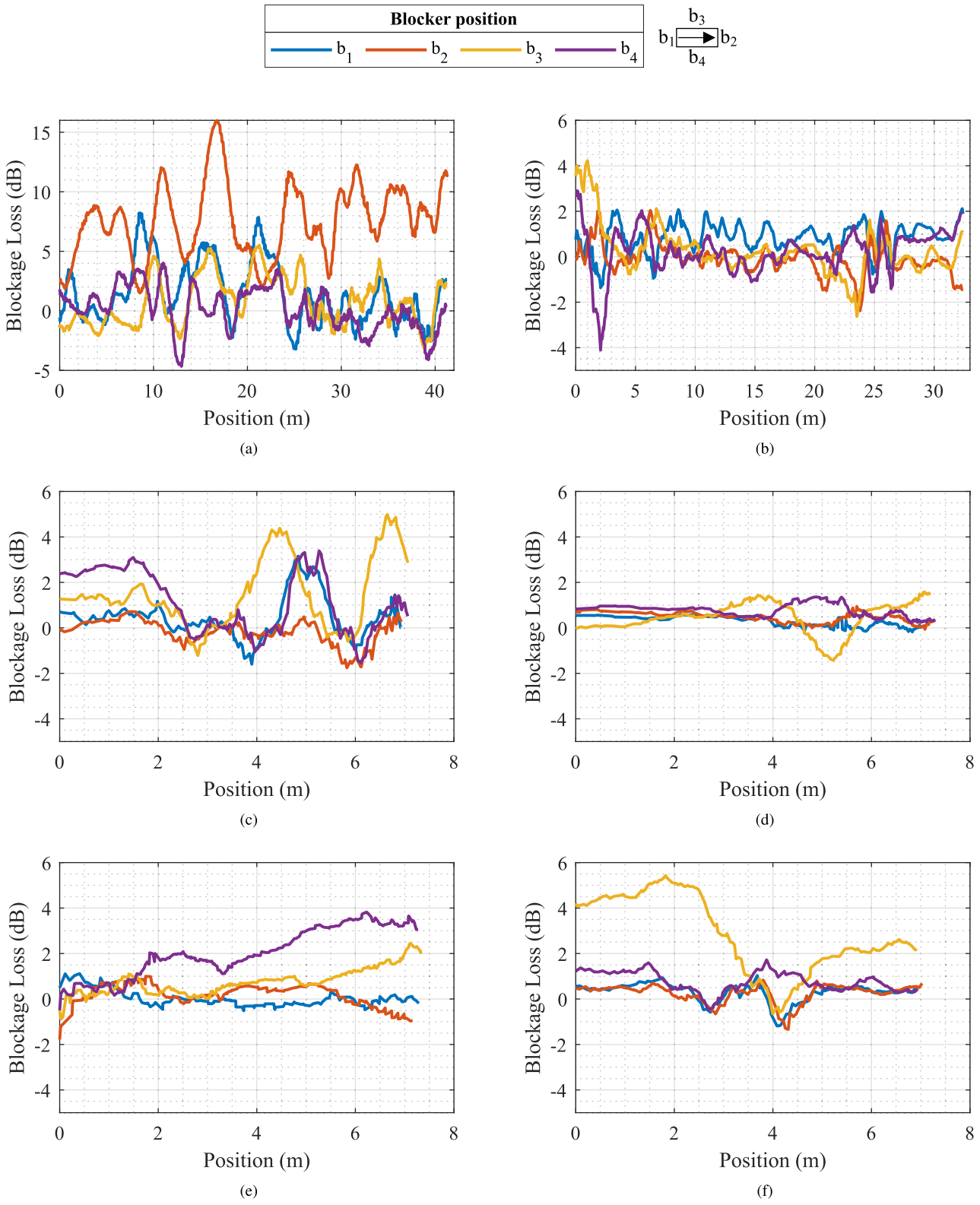

Fig. 6. Measured human blockage loss along the tracks in scenario 1. (a) Track 1. (b) Track 2. (c) Track 3. (d) Track 4. (e) Track 5. (f) Track 6.

tracks 5 and 6. The largest blockage occurs at the end of track 5 and at the start of track 6, where b_4 and b_3, respectively, block the most DPs coming from the long corridor at the bottom of Fig. 2, which results in a 3–5 dB blockage loss. Reflections from the meeting room next to this track limit the blockage loss here.

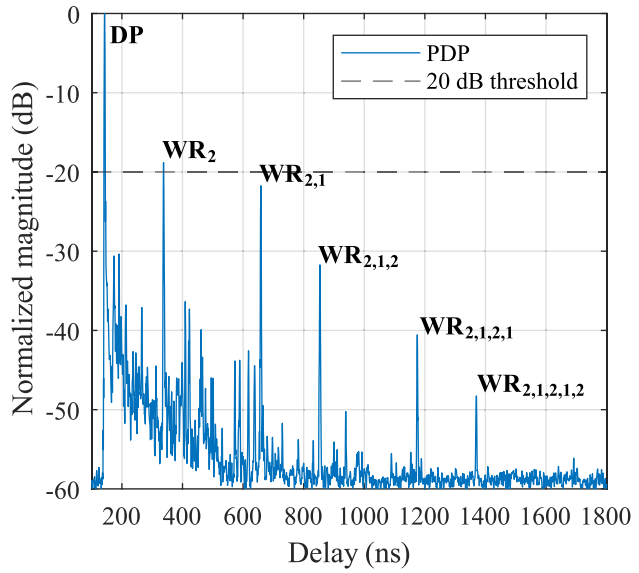

Fig. 7. Example of a PDP, $p^{tot}(\tau)$, in the middle of track 1 for b_0, which shows several distinct paths WR_r that are established via reflections from the windows w_1 and w_2.

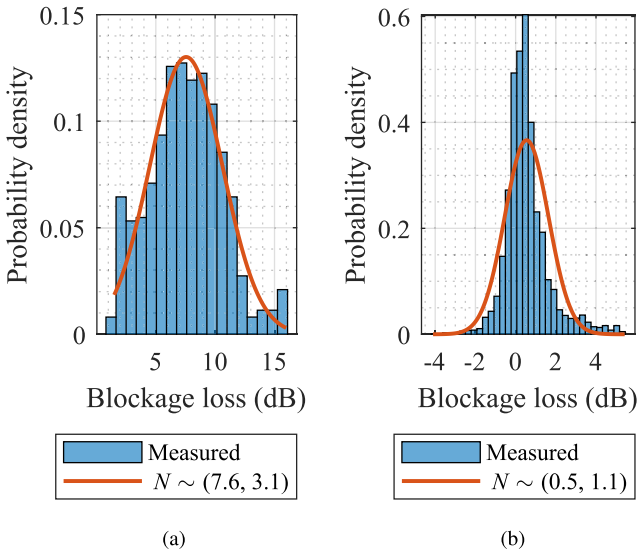

Fig. 8. Blockage loss distributions of scenario 1. (a) Category A: LOS with DP blocked. (b) Category B: NLOS with potential human blocker.

B. Statistics of Human Blockage Loss

Probability distributions can provide a general overview of the measured human blockage loss and can be used for comparison to results in the literature. The blockage loss can be generalized into two categories: A) LOS with DP blocked and B) NLOS with potential human blocker. Category A can be compared to the human blockage loss models and measurements available in the literature to show the impact of the multipath environment in case of a blocked DP in an LOS. Category B shows how much blockage loss a potential human blocker causes in an NLOS channel, where the direction of arrival of the strongest path is unknown. The corresponding probability distributions are shown in Fig. 8, including their least-squares fit to the normal distribution $N \sim (\mu, \sigma)$.

The probability distribution in Fig. 8(a) of an LOS with the DP blocked is obtained from the measurements of b_2 along track 1. It has a mean blockage loss of 7.6 dB and a standard deviation of 3.1 dB, where the normal distribution underestimates the maximum blockage occurrences. The measured blockage ranges between 2 and 16 dB. These human blockage results can be compared to the results reported in [8], which show a 20–30 dB blockage loss at 28 GHz for a human blocker at 0.6–0.8 m from a 20 dBi antenna. No direct comparison can be made to the results reported in [6], [7], [9], and [12] due to the use of different frequencies or different distances between the blocker and the antenna, but these papers also report a larger human blockage loss of typically 10–30 dB. In these papers, the effect of multipaths is limited by using short distances between the Tx and Rx antennas or by measuring in an open space. The results presented in this article thus show that along the measured indoor LOS track, the multipath environment highly limits the blockage loss in case of a blocked DP by a human blocker close by an MT.

The probability distribution of human blockage loss in case of an NLOS with a potential human blocker is shown in Fig. 8(b), which includes the measurements of blocker positions b_1–b_4 along tracks 2–6. The normal distribution fit is provided for reference, which underestimates the 0–1 dB and 3–5 dB blockage loss occurrences. These results show that the potential human blocker in an NLOS environment results in a very limited blockage loss with a mean of 0.5 dB and a maximum of 5 dB. The measured human blockage loss in an NLOS environment, which typically contains more MPCs than an LOS environment, is thus highly limited by the rich multipath environment for a human blocker close by an MT.

C. Impact of Human Blockage on Close-In Path Loss Model

The CI-model is fitted to the measured PL^{tot} of scenario 1 for all blocker positions and tracks to show how the different blocker positions change the statistics of the measured channels. Using a close-in distance of 1 m, the CI-model can be defined as

$$PL^{CI}(d) = 20\log_{10}\left(\frac{4\pi f}{c}\right) + 10\, n \log_{10}(d) + \chi_{\sigma_{SF}} \qquad (7)$$

where d is the distance between the Tx and the Rx, f is the carrier frequency, c is the speed of light, n is the PL exponent, and $\chi_{\sigma_{SF}}$ is a normally distributed random variable with zero mean and standard deviation σ_{SF}, also known as the shadow factor [25].

n and σ_{SF} of the CI-model fits are given in Table II and compared to the unblocked case b_0. Blocker b_2 at LOS track 1, which blocks the DP, increases n from 1.9 to 2.4 and σ_{SF} from 3.8 to 4.2 dB. The increase in n is most significant and shows that blockage of the DP significantly changes the channel statistics in an LOS environment. The largest change in σ_{SF} occurs for b_1 along track 1, where σ_{SF} increases from 3.8 to 4.5 dB. This is caused by blockage of WR_2, which then cannot compensate for losses due to multipath fading in the DP. Blockers b_1–b_4 along NLOS tracks 2–6 result in a maximum change of 0.1 in n and 0.3 dB in σ_{SF}. The channel

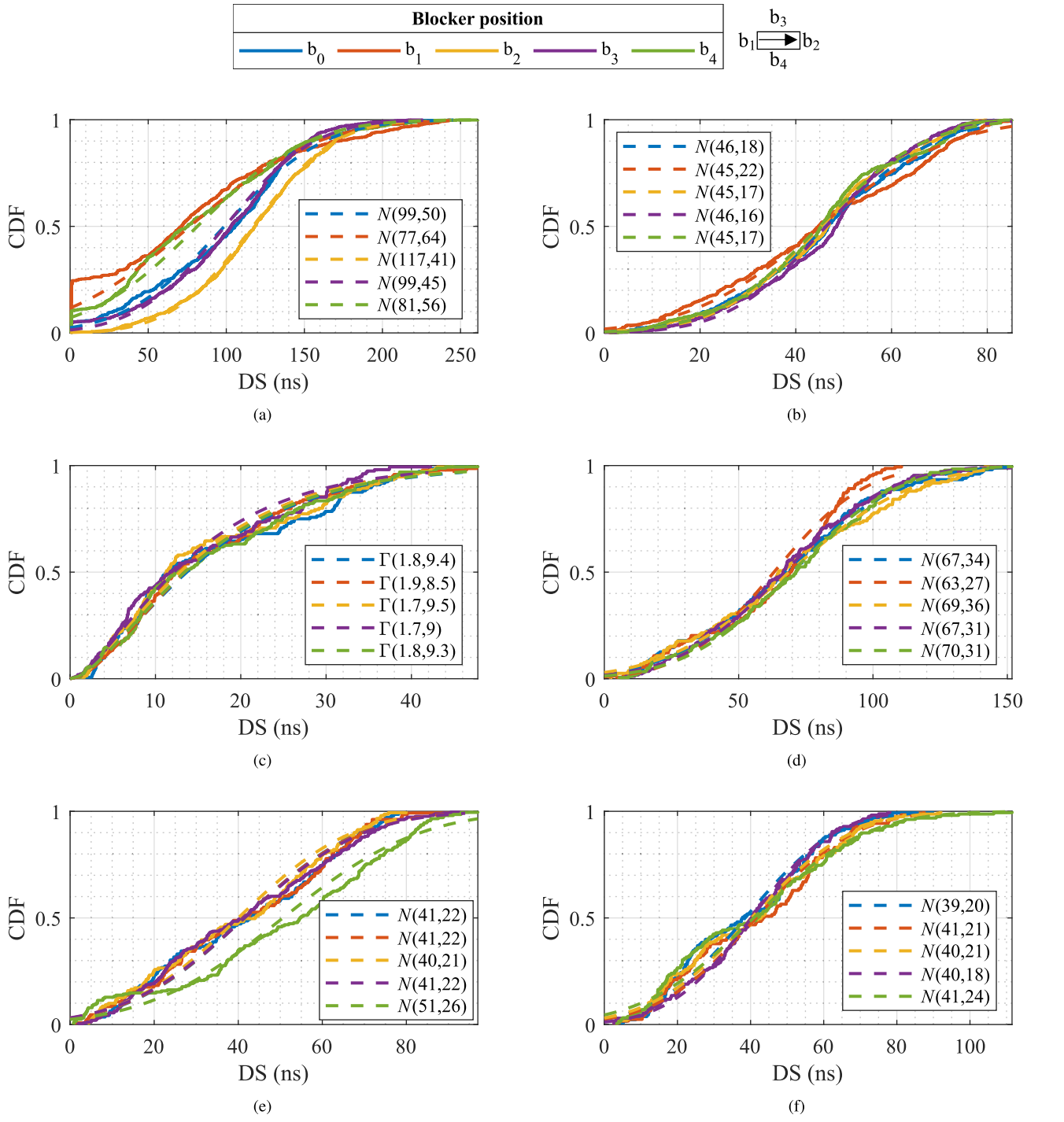

Fig. 9. Measured cdfs (solid lines) of DS^{tot} along the tracks in scenario 1 for the blocker positions b_0–b_4 and corresponding distributions (dashed lines). (a) Track 1. (b) Track 2. (c) Track 3. (d) Track 4. (e) Track 5. (f) Track 6.

statistics are thus not significantly altered by a human blocker close by an MT in the measured NLOS channels.

D. Delay Spread

Another important large-scale parameter that can be affected by human blockage is the DS. DS^{tot} for all blocker positions of each track is compared via the respective cumulative distribution functions (cdfs). The cdfs of the measured DS^{tot} are plotted as solid lines in Fig. 9 for tracks 1–6. The corresponding normal or gamma distributions are depicted by dashed lines, where the gamma distribution is given as $\Gamma(k, \theta)$. The cdf is zero for DS smaller than zero by the definition of DS, so all negative values obtained from these distributions should be equated to zero when using these distributions. DS^{tot} of LOS track 1 is large due to the WR_r paths, which have large propagation delays. Blocker b_2 mainly blocks the DP, which increases the corresponding DS^{tot}. Blocker position

TABLE II

CI-MODEL PARAMETERS OF PL^{tot} FOR ALL BLOCKER POSITIONS ALONG EACH TRACK IN SCENARIO 1, WITH σ_{SF} IN dB

Track	b_0		b_1		b_2		b_3		b_4	
	n	σ_{SF}	n	σ_{SF}	n	σ_{SF}	n	σ_{SF}	n	σ_{SF}
1	1.9	3.8	2.0	4.5	2.4	4.2	2.0	3.9	1.9	3.7
2	3.0	2.8	3.0	3.1	3.0	2.7	3.0	2.2	3.0	2.9
3	2.6	4.0	2.6	3.9	2.6	4.1	2.7	4.1	2.7	4.3
4	3.2	1.5	3.2	1.6	3.3	1.7	3.3	1.5	3.3	1.3
5	2.8	2.7	2.8	2.6	2.8	2.8	2.8	2.4	2.9	2.5
6	2.7	2.7	2.7	2.7	2.7	2.9	2.9	2.9	2.7	2.8

TABLE III

PERCENTAGE (%) OF THE MEASUREMENT POINTS THAT EACH TX BEAM IS OPTIMUM ALONG A TRACK AND ITS PERCENTAGE OF THE TOTAL PATH GAIN, BOTH FOR THE UNBLOCKED CASE b_0

Track	% optimum			% path gain		
	Tx_1	Tx_2	Tx_3	Tx_1	Tx_2	Tx_3
1	0	100	0	1	99	0
2	14	53	33	22	44	35
3	71	10	19	59	14	28
4	0	100	0	4	92	4
5	0	100	0	13	81	5
6	0	100	0	12	84	4

b_1 decreases DS^{tot} by blocking the WR_r paths arriving from the back. Blocker b_4 also shows a lower DS^{tot}, which can also be caused by blockage of WR_r paths. DS^{tot} of this LOS track is thus significantly affected by human blockage, which is also visible by the change in mean value of the normal distributions.

Fig. 9(a)–(f) shows the DS^{tot} cdfs for the NLOS tracks 2–6. Track 3 has a relatively small DS^{tot} because it is shielded from the large open area and long corridors by the elevators and is best represented by a gamma distribution. The most significant impact of a blocker on DS^{tot} is along track 5 for blocker position b_4, where the average DS^{tot} is increased by a blocker on the right, blocking paths from the corridor at which beam Tx_2 is pointed. The overall impact of human blockage on the DS^{tot} of the NLOS tracks is small and typically negligible, which is also shown by the limited differences in the normal and gamma distribution parameters of the different blocker positions.

E. Impact of Human Blockage on Directional Channels

The results presented above show that the impact of human blockage on the aggregate channel is mitigated by the multipath nature of this channel. However, the adoption of directional antennas in mm-wave communication systems limits the number of available MPCs at a given time. Beam steering or switching is then needed at both the AP and MT to point the antenna beams in the optimum directions. The beam switching or steering methods applied, as well as the antenna beamwidths, will affect the impact of human blockage on directional channels.

TABLE IV

PERCENTAGE (%) OF MEASUREMENT POINTS THAT HAVE A DIFFERENT OPTIMUM BEAM THAN THEIR PRECEDING MEASUREMENT POINT FOR EACH BLOCKER POSITION, INDICATING A CHANGE IN OPTIMUM TX BEAM

Track	b_0	b_1	b_2	b_3	b_4
1	0	0	0	0	0
2	14	8	14	12	13
3	23	23	22	32	27
4	0	0	0	0	0
5	0	0	1	1	0
6	0	0	0	0	0

The effect of Tx beam switching on the measured human blockage loss is investigated for scenario 1 to show whether AP beam switching could mitigate human blockage. The unblocked case of blocker position b_0 is used as a reference. The contribution of each beam Tx_t is quantized for b_0 in order to show how much these beams contribute to the aggregate channel. The percentage of measurement points, for which each beam Tx_t is optimum, is calculated for each track, where the beam with the lowest PL_t is considered optimum. In addition, the percentage of the total path gain that each Tx beam contributes to the channel is calculated for b_0 along each track as

$$\%\ \text{path gain} = \left(\frac{1}{M_{tr}} \sum_{m=1}^{M_{tr}} \frac{10^{-\frac{PL_t(m)}{10}}}{\sum_t 10^{-\frac{PL_t(m)}{10}}} \right) \times 100\% \qquad (8)$$

where M_{tr} is the total number of measurement points along the track. The calculated percentages are given in Table III. Beam Tx_2 is optimum along the entire tracks 1 and 4–6 with over 80% of the total path gain established via beam Tx_2. This shows that the average contribution of Tx_1 and Tx_3 is small along these tracks. Each of the three Tx beams is optimum along part of tracks 2 and 3, and the percentage path gain along these tracks is more evenly divided over these beams. Thus, beam switching is required along tracks 2 and 3 to maintain the lowest PL_t in the unblocked case.

Table IV shows the percentage of measurement points that have a different optimum beam than their preceding measurement points for all blocker positions. Switching to a

different beam would thus result in a lower PL_t for this percentage of measurements. For reference b_0, when no blocker is present in the channel, 0% of optimum beam changes occur for tracks 1 and 4–6 because beam Tx_2 is always optimum here. Beam Tx_2 remains optimum for almost all measurements along these tracks when a blocker is present in the channel, with 0%–1% changes in optimum beam. Thus, in the measured human blockage scenario, Tx beam switching cannot improve the channel when there is one dominant beam in the unblocked channel, which provides over 80% of the total path gain; 14% and 23% of changes in optimum beam occur along unblocked tracks 2 and 3, respectively. Blocker position b_1 reduces the number of optimum beam changes along track 2 to 8%. Blocker positions b_3 and b_4 increase the percentage of optimum beam changes along track 3 to 32% and 27%, respectively, by mainly blocking the paths from Tx_1. Thus, human blockage in the measured scenario can both slightly increase or decrease the number of optimum Tx beam changes when there are multiple Tx beams that contribute to the unblocked channel, but the overall impact of Tx beam switching is limited.

It is expected that Rx beam switching will be more important to limit human blockage loss because both scatterers and human blockers are in general closer to the MT than AP. No angle-of-arrival information is obtained in the measurement campaign discussed in this article. However, some comparisons between the time of arrivals and the physically possible paths between the Tx and the Rx can be made. In case of LOS track 1, WR_2 is sometimes stronger than the DP, thus requiring a 180° beam change to minimize the PL. For track 3, all three beams are optimum along part of the track, which will require Rx beam switching to minimize the PL.

V. Results of Scenario 2: Static MT With One or Multiple Human Blockers

In contrast to scenario 1, scenario 2 shows the impact of one or multiple human blockers further away from a static MT. The corresponding human blockage loss is discussed for both an LOS and NLOS location. The use of a static MT allows for direct comparison between the PDPs of blocked and unblocked measurements. The impact of human blockage on the DS for this scenario is shown at the end of this section.

A. Human Blockage Loss

For scenario 2, the human blockage loss is calculated as

$$\mathrm{HBL}(m) = \mathrm{PL}^{\mathrm{tot}}(m) - \mathrm{PL}^{\mathrm{tot}}_{\mathrm{unblocked}} \tag{9}$$

where $\mathrm{PL}^{\mathrm{tot}}(m)$ is the PL for measurement point m and $\mathrm{PL}^{\mathrm{tot}}_{\mathrm{unblocked}}$ is the PL of the static aggregate channel without a human blocker. $\mathrm{PL}^{\mathrm{tot}}_{\mathrm{unblocked}}$ is 97.5 dB for s_{LOS} and 101.6 dB for s_{NLOS}. Five measurement points per second are taken. The number of measurement points for every measurement set (see Fig. 5 for corresponding tracks and areas) is given in Table V, as well as the minimum, mean, and maximum human blockage loss.

TABLE V

Minimum, Mean, and Maximum Measured Human Blockage Loss (in dB) and the Number of Measurement Points for the Various Measurement Sets in Scenario 2

measurement set	# measurement points	blockage loss (dB)		
		min	mean	max
$1HB_{LOS}$-OT	721	-1.0	0.2	0.9
$1HB_{LOS}$-PT	481	-3.5	1.7	7.5
MHB_{LOS}	1129	-5.0	2.1	9.5
$1HB_{NLOS}$-BT	200	-2.4	0.2	2.0
$1HB_{NLOS}$-GT	154	-1.6	0.0	0.9
$1HB_{NLOS}$-RT	202	-0.5	0.1	0.5
MHB_{NLOS}	1096	-2.1	0.3	2.3

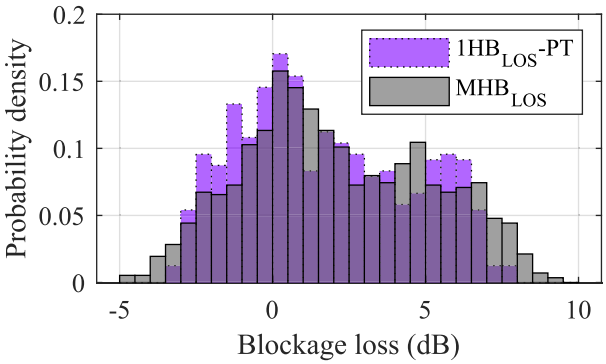

Fig. 10. Blockage loss distributions of $1HB_{LOS}$-PT and MHB_{LOS} at s_{LOS} for scenario 2.

1) LOS Location s_{LOS}: There is an LOS between the Tx and the Rx when the Rx is positioned at s_{LOS} and only beam Tx_2 contributes to the channel at this location. $1HB_{LOS}$-OT, where the single potential blocker is behind the Rx and thus not within the DP, results in a negligible ±1 dB blockage loss. Analysis of the corresponding PDPs (not shown) reveals that the DP remains constant for all $1HB_{LOS}$-OT measurement points, but the magnitude of WR_2 fluctuates due to the human blocker, which results in small fluctuations in blockage loss.

Fig. 10 shows the blockage loss distribution of $1HB_{LOS}$-PT, where the blocker is in the area between the Tx and the Rx. Part of this track is not directly in between the Tx and Rx, which explains the low absolute blockage loss occurrences. However, the blockage loss neither exceeds 7.5 dB when the blocker is directly in between the Tx and the Rx, blocking the LOS. The blockage loss is low compared to the measured blockage loss of 15–30 dB for case 1 in [8], where a human blocker walks between two directional antennas that are in LOS and separated by 3.6 m. The measurements presented here have a much larger Tx–Rx distance and include an omnidirectional Rx antenna, which allows MPCs from the floor, ceiling, and walls to contribute to the channel and limit the blockage loss.

The blockage loss distribution of MHB_{LOS} with six potential blockers in the gray area around s_{LOS} is also shown in Fig. 10. There was always one person in the area between the Tx and the Rx, more than one person for 90% and all six people for

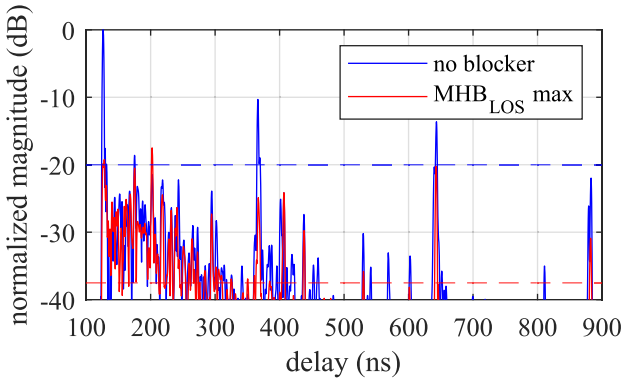

Fig. 11. Comparison of PDPs in case of no blocker and the maximum blockage of MHB_{LOS} at s_{LOS} for scenario 2. The dashed lines depict the 20 dB thresholds.

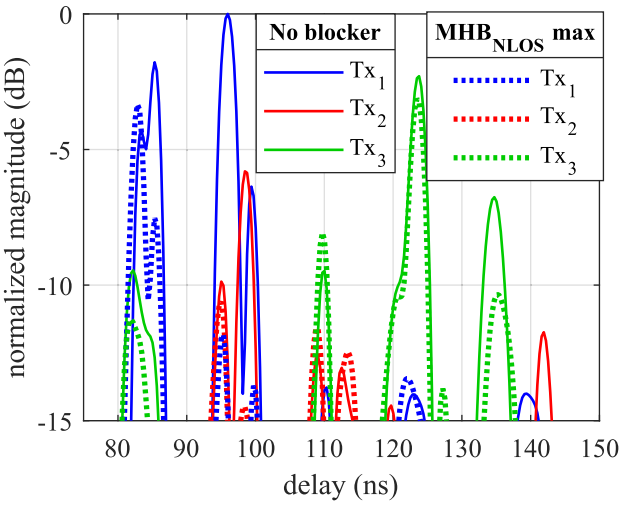

Fig. 12. PDPs for beams Tx_1, Tx_2, and Tx_3 in case of no blockage at s_{NLOS}, compared to the maximum blockage of MHB_{NLOS} for scenario 2.

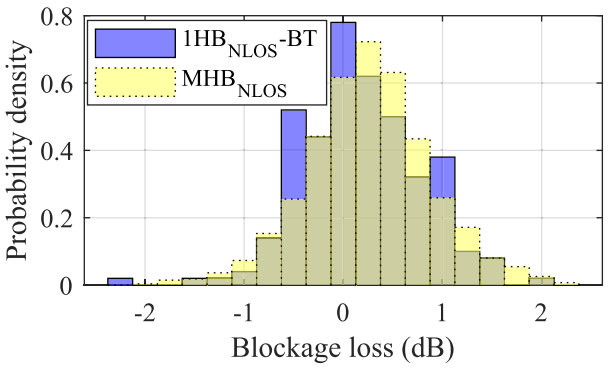

Fig. 13. Probability density of blockage loss at s_{NLOS} of $1HB_{NLOS}$-BT and MHB_{NLOS} for scenario 2.

14% of the measurements. The additional human blockers only result in a slight increase in mean and maximum blockage loss compared to $1HB_{LOS}$-PT. Both the $1HB_{LOS}$-PT and MHB_{LOS} blockage loss distributions exhibit a bimodality. One mode is visible around 0 dB, where the blockers cause a change in fading. A second mode is present around 5 dB, which occurs due to blockage of the main paths. The maximum blockage loss of 9.5 dB occurred when only three people were in the area between the Tx and the Rx. The PDP of this measurement is shown in Fig. 11 with the PDP of the static unblocked channel for comparison. The PDP of maximum blockage is shifted -1.8 ns to align its DP peak to the unblocked DP peak. The corresponding 20 dB thresholds are depicted by dotted lines. The DP is attenuated with 19 dB by the blockers compared to the unblocked DP, while the blockage loss is only increased by 9.5 dB. This is due to the contribution of other MPCs in the channel within the 20 dB dynamic range. The multipath nature of the channel thus reduces the blockage loss by 10 dB for this measurement.

2) NLOS Location s_{NLOS}: The second static MT location s_{NLOS} is an NLOS position in a hallway next to the elevators, as shown in Fig. 5. The PL for the separate channels, PL_1, PL_2, and PL_3, is 104.6, 109, and 106.7 dB, respectively, which shows that all three Tx beams significantly contribute to the channel. Fig. 12 shows the corresponding normalized PDPs (solid lines) for the window 75–150 ns, which contains the strongest paths. The peaks centered around 85 ns are the most DPs via the corridor that Tx_1 points at. The peak of Tx_3 at 85 ns is due to radiation of Tx_3 outside of its HPBW, in the pointing direction of Tx_1. The strongest path at 96 ns originates from Tx_1 and is a reflected path via the elevator. This path is thus stronger than the more DP from Tx_1. The three strongest paths of Tx_3 between 110 and 135 ns are via the corridor that Tx_3 points at and contain a different number of bounces between the metal fire doors and elevator around s_{NLOS}.

The two strongest paths from Tx_1 are not blocked by the potential blocker in $1HB_{NLOS}$-GT and $1HB_{NLOS}$-RT, which results in a negligible blockage loss of less than 1 dB (see Table V). In $1HB_{NLOS}$-BT, the strongest paths are potentially blocked by the human blocker, but this blocker only causes a maximum blockage loss of 2 dB. The corresponding blockage loss distribution is shown in Fig. 13. The human blocker slightly changes the multipath fading but does not add significant blockage loss here.

In the MHB_{NLOS} experiment, three people are asked to walk randomly around s_{NLOS} in the yellow area in Fig. 5. The blockage loss probability distribution for MHB_{NLOS} is also shown in Fig. 13. The maximum measured blockage loss is 2.3 dB, which shows that severe blockage is prevented by the multipath environment. The maximum blockage occurred when one person was in the middle of the corridor that Tx_1 is pointed at and another person was directly in between the Rx and the elevator. The corresponding PDPs for the three Tx beams are plotted in Fig. 12 (dotted lines). The strongest MPC at 96 ns is attenuated by 12 dB compared to the no blocker case. This reflected path from the elevator is blocked by the person standing in between the elevator and the Rx. The second potential blocker in the corridor that Tx_1 is pointed at possibly contribute to the attenuation of the MPC at 96 ns too. The magnitude of the two paths around 85 ns is also changed due to this blocker. The attenuation of the strongest MPC from Tx_1 is compensated by other MPCs from mainly Tx_1 and Tx_3,

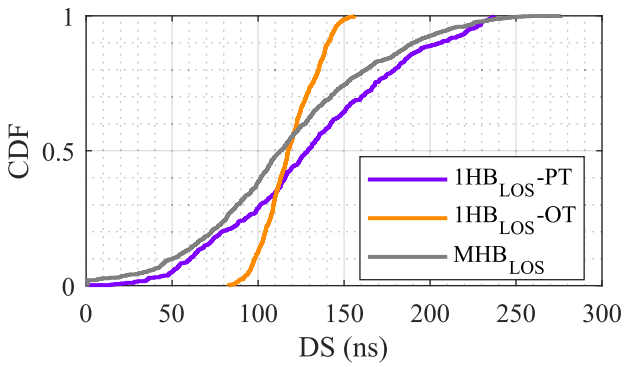

Fig. 14. CDFs of DS^{tot} for measurements at s_{LOS} for scenario 2.

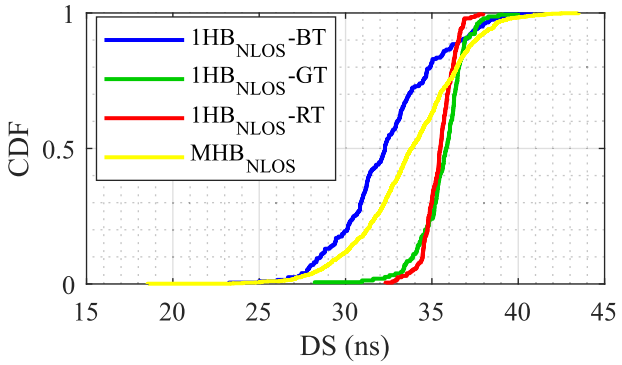

Fig. 15. CDFs of DS^{tot} for measurements at s_{NLOS} for scenario 2.

resulting in a 2.3 dB human blockage loss opposed to 12 dB. This shows that the effect of human blockage can be reduced by a rich multipath environment in an NLOS location.

B. Delay Spread

The cdfs for the measurements of DS^{tot} at s_{LOS} are shown in Fig. 14. DS^{tot} in case of the static channel with no blocker is 112 ns. DS^{tot} is mainly determined by the magnitude of the WR_r paths relative to the DP. $1HB_{LOS}$-OT results in relatively small changes in DS^{tot}, due to (partial) blockage of WR_r paths arriving from the back. DS^{tot} varies between 1 and 237 ns for $1HB_{LOS}$-PT, where the minimum DS^{tot} occurs when there are no MPCs within 20 dB of the DP and the maximum occurs when the DP is severely blocked. MHB_{LOS} shows a lower DS^{tot} compared to $1HB_{LOS}$-PT due to higher blockage of WR_r paths when multiple blockers are in the channel. For s_{LOS}, a similarly large variation in DS^{tot} can thus be observed as for LOS track 1 in scenario 1 due to (partial) blockage of the DP and WR_r paths.

Fig. 15 shows the cdfs of DS^{tot} for NLOS location s_{NLOS}. DS^{tot} in case of no blockage is 36 ns. The variation in DS^{tot} is small for most measurements along $1HB_{NLOS}$-GT and $1HB_{NLOS}$-RT. $1HB_{NLOS}$-BT and MHB_{NLOS} show a small reduction in median DS^{tot} and a larger spread. However, the absolute variation in DS^{tot} for s_{NLOS} is small.

VI. Conclusion

The impact of human blockage on the dynamic indoor multipath channel at 27 GHz is investigated in this article. The effect of one human blocker close by a dynamic MT is shown in scenario 1. In case of an LOS with its DP blocked, the measured human blockage loss ranges between 2 and 16 dB, which is significantly lower than the 10–30 dB human blockage loss that is typically reported in the literature, where the contribution of MPCs other than the DP is neglected or minimized. Compared to the unblocked case, the PL exponent is increased from 1.9 to 2.4 and the DS is increased as well. A potential human blocker close by a dynamic MT in the measured NLOS channels results in a -4 to 5 dB blockage loss, which can be mainly attributed to changes in multipath fading. The changes in PL exponent and DS are negligible for most blocker positions in these NLOS channels. For both the LOS and NLOS aggregate channels, which approximate the omnidirectional channel, the multipath environment can thus highly limit the human blockage loss when the blocker is close by the MT. In case of directional channels, it is shown that the impact of Tx beam switching on human blockage loss is limited.

Measurement scenario 2 shows the effect of one or multiple potential human blockers further away from a static MT. In case of one human blocker, the maximum measured human blockage loss is 7.5 dB in the LOS channel and 2 dB in the NLOS channel. The human blockage loss distribution does not significantly change for multiple human blockers. Comparison of the PDPs in case of no and maximum blockage shows that the multipath nature of the channels also highly limits the human blockage loss in this measurement scenario.

Acknowledgment

This work is part of the Flagship Telecom collaboration between KPN and the Eindhoven University of Technology. The authors would like to thank their colleagues who took part in the multiple human blocker measurements.

References

[1] P. Cerwall, A. Lundvall, P. Jonsson, S. Carson, and R. Möller, "Ericsson mobility report," Ericsson, Stockholm, Sweden, Tech. Rep. EAB-20:009174, 2020.

[2] Internation Telecommunications Union, *World Radiocommunication Conference 2019 (WRC-19) Final Acts*, ITU Publications, 2020.

[3] European Commission, *Commission Implementing Decision (EU) 2019/784 of 14 May 2019 on Harmonisation of the 24,25-27,5 GHz Frequency Band for Terrestrial Systems Capable of Providing Wireless Broadband Electronic Communications Services in the Union*, document 3450, 2019.

[4] *Commission Implementing Decision (EU) 2020/590 of 24 April 2020 Amending Decision (EU) 2019/784 as Regards an Update of Relevant Technical Conditions Applicable to the 24,25-27,5 GHz Frequency Band*, document 2542, 2020.

[5] S. Rangan, T. S. Rappaport, and E. Erkip, "Millimeter-wave cellular wireless networks: Potentials and challenges," *Proc. IEEE*, vol. 102, no. 3, pp. 366–385, Feb. 2014.

[6] U. T. Virk and K. Haneda, "Modeling human blockage at 5G millimeter-wave frequencies," *IEEE Trans. Antennas Propag.*, vol. 68, no. 3, pp. 2256–2266, Mar. 2020.

[7] G. R. MacCartney, S. Deng, S. Sun, and T. S. Rappaport, "Millimeter-wave human blockage at 73 GHz with a simple double knife-edge diffraction model and extension for directional antennas," in *Proc. IEEE 84th Veh. Technol. Conf. (VTC-Fall)*, Sep. 2016, pp. 1–6.

[8] W. Qi, J. Huang, J. Sun, Y. Tan, C.-X. Wang, and X. Ge, "Measurements and modeling of human blockage effects for multiple millimeter wave bands," in *Proc. 13th Int. Wireless Commun. Mobile Comput. Conf. (IWCMC)*, Jun. 2017, pp. 1604–1609.

[9] Q. Wang, X. Zhao, S. Li, M. Wang, S. Sun, and W. Hong, "Attenuation by a human body and trees as well as material penetration loss in 26 and 39 GHz millimeter wave bands," *Int. J. Antennas Propag.*, vol. 2017, Mar. 2017, Art. no. 2961090.
[10] J. S. Lu, D. Steinbach, P. Cabrol, and P. Pietraski, "Modeling human blockers in millimeter wave radio links," *ZTE Commun.*, vol. 10, no. 4, pp. 23–28, Dec. 2012.
[11] G. R. MacCartney, T. S. Rappaport, and S. Rangan, "Rapid fading due to human blockage in pedestrian crowds at 5G millimeter-wave frequencies," in *Proc. IEEE Global Commun. Conf. (GLOBECOM)*, Dec. 2017, pp. 1–7.
[12] P. Karadimas, B. Allen, and P. Smith, "Human body shadowing characterization for 60-GHz indoor short-range wireless links," *IEEE Antennas Wireless Propag. Lett.*, vol. 12, pp. 1650–1653, 2013.
[13] M. Peter *et al.*, "Analyzing human body shadowing at 60 GHz: Systematic wideband MIMO measurements and modeling approaches," in *Proc. 6th Eur. Conf. Antennas Propag. (EUCAP)*, Mar. 2012, pp. 468–472.
[14] P. Paschalidis, M. Wisotzki, A. Kortke, W. Keusgen, and M. Peter, "A wideband channel sounder for car-to-car radio channel measurements at 5.7 GHz and results for an urban scenario," in *Proc. IEEE 68th Veh. Technol. Conf.*, Sep. 2008, pp. 1–5.
[15] P. B. Papazian *et al.*, "Calibration of millimeter-wave channel sounders for super-resolution multipath component extraction," in *Proc. 10th Eur. Conf. Antennas Propag. (EuCAP)*, Apr. 2016, pp. 1–5.
[16] S. Sun, G. R. MacCartney, M. K. Samimi, and T. S. Rappaport, "Synthesizing omnidirectional antenna patterns, received power and path loss from directional antennas for 5G millimeter-wave communications," in *Proc. IEEE Global Commun. Conf. (GLOBECOM)*, Dec. 2014, pp. 1–7.
[17] M. Boban *et al.*, "Multi-band vehicle-to-vehicle channel characterization in the presence of vehicle blockage," *IEEE Access*, vol. 7, pp. 9724–9735, 2019.
[18] S. Hur, Y.-J. Cho, J. Lee, N.-G. Kang, J. Park, and H. Benn, "Synchronous channel sounder using horn antenna and indoor measurements on 28 GHz," in *Proc. IEEE Int. Black Sea Conf. Commun. Netw. (BlackSeaCom)*, May 2014, pp. 83–87.
[19] C. U. Bas *et al.*, "Real-time millimeter-wave MIMO channel sounder for dynamic directional measurements," *IEEE Trans. Veh. Technol.*, vol. 68, no. 9, pp. 8775–8789, Sep. 2019.
[20] S. Salous, S. M. Feeney, X. Raimundo, and A. A. Cheema, "Wideband MIMO channel sounder for radio measurements in the 60 GHz band," *IEEE Trans. Wireless Commun.*, vol. 15, no. 4, pp. 2825–2832, Apr. 2016.
[21] G. R. MacCartney and T. S. Rappaport, "A flexible millimeter-wave channel sounder with absolute timing," *IEEE J. Sel. Areas Commun.*, vol. 35, no. 6, pp. 1402–1418, Jun. 2017.
[22] R. Müller *et al.*, "Simultaneous multi-band channel sounding at mm-wave frequencies," in *Proc. 10th Eur. Conf. Antennas Propag. (EuCAP)*, Apr. 2016, pp. 1–5.
[23] ITU-R, *Multipath Propagation and Parameterization of Its Characteristics*, Recommendation, document ITU-R P.1407-7, 2019.
[24] T. S. Rappaport *et al.*, "Millimeter wave mobile communications for 5G cellular: It will work!" *IEEE Access*, vol. 1, pp. 335–349, 2013.
[25] T. S. Rappaport, *Wireless Communications: Principles and Practice*, vol. 2. Upper Saddle River, NJ, USA: Prentice-Hall, 1996.

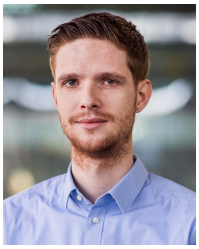

Robbert Schulpen received the M.Sc. degree *(cum laude)* in electrical engineering from the Eindhoven University of Technology, Eindhoven, The Netherlands, in 2017, where he is currently pursuing the Ph.D. degree in electrical engineering.

His research interests include millimeter-wave metrology, millimeter-wave channel characterization, and channel sounder design, calibration, and verification.

Laurens A. Bronckers (Member, IEEE) received the M.Sc. degree *(cum laude)* in electrical engineering from the Eindhoven University of Technology (TU/e), Eindhoven, The Netherlands, in 2015, and the Ph.D. degree *(cum laude)* in electrical engineering from the Electromagnetics Group, TU/e, in 2019, with a focus on design and measurement techniques for the next-generation integrated antennas.

In 2018, he was a Visiting Researcher with NIST, Boulder, CO, USA, where he was involved in antenna measurements in reverberation chambers. Since 2019, he has been an Assistant Professor of metrology for antennas and wireless systems with TU/e. His research interests include antenna measurements in reverberation and anechoic chambers, channel sounding and emulation, and RF material characterization.

A. Bart Smolders (Senior Member, IEEE) received the Ph.D. degree in electrical engineering from the Eindhoven University of Technology (TU/e), Eindhoven, The Netherlands, in 1994.

He is an expert in smart antenna systems and worked at TNO, Hague, The Netherlands, THALES, Hengelo, The Netherlands, ASTRON, Dwingeloo, The Netherlands, and NXP semiconductors, Nijmegen, The Netherlands. Since 2010, he has been a full-time Professor with the Electromagnetics Group, TU/e, with a special interest in smart antenna systems and applications. He currently leads several large research projects in the area of integrated antenna systems for 5G/6G wireless communications and radar. Next to his research activities, he is the Dean of the Electrical Engineering Department, TU/e.

Ulf Johannsen (Member, IEEE) received the Dipl.-Ing. degree in communications engineering from the Hamburg University of Technology (TUHH), Hamburg, Germany, in 2009, and the Ph.D. degree in electrical engineering from the Eindhoven University of Technology (TU/e), Eindhoven, The Netherlands, in 2013.

From 2013 to 2016, he was a Senior Systems Engineer with ATLAS ELEKTRONIK GmbH, Bremen, Germany, where he was a System Designer and an Engineering Manager of autonomous underwater vehicle (AUV) systems with sonar payloads. Since 2016, he has been with the Electromagnetics Group, Department of Electrical Engineering, TU/e, where he is currently an Associate Professor. His research interest includes integrated antenna systems.

Dr. Johannsen was the Coordinator of the TU/e's Centre for Wireless Technologies' (CWTe) Ultra-High Data-Rate Programme and is the Chairperson of the IEEE Benelux Joint AP/MTT Chapter. Moreover, he is a member of the Advisory Board of the Chip Integration Technology Centre (CITC), Nijmegen, The Netherlands.